

Instanton-Induced Processes in Deep-Inelastic Scattering*

A. Ringwald and F. Schrempp

Deutsches Elektronen-Synchrotron DESY, Hamburg, Germany

Abstract

We present a status report of our systematic theoretical and phenomenological study of QCD-instanton induced processes in deep-inelastic scattering. We show that this regime plays a distinguished rôle for studying manifestations of QCD-instantons, since the typical hard momentum scale Q provides a dynamical infrared cutoff for the instanton size $\rho \lesssim \mathcal{O}(1/Q)$. For deep-inelastic scattering at HERA, we present a preliminary theoretical estimate of the total instanton-induced cross-section (subject to appropriate kinematical cuts). It is surprisingly large, in the $\mathcal{O}(1 - 100)$ pb range, albeit still uncertain. We report on our investigation of the discovery potential for instanton-induced events at HERA by means of a Monte Carlo event generator. It is based on a detailed study of the characteristic signatures of the final state, like a large total transverse energy, $E_T = \mathcal{O}(20)$ GeV, a large multiplicity, $n = \mathcal{O}(25)$, and a flavour-democratic production of hadrons. A combination of event shape information with searches of K^0 mesons, muons, and multiplicity cuts might help to discriminate further the QCD-instanton induced processes from the standard perturbative QCD background.

*To be published in: *Quarks '96*, Proc. IXth International Seminar, Yaroslavl, Russia, May 5-11, 1996.

1 Introduction

The Standard Model of strong (QCD) and electro-weak (QED) interactions is remarkably successful. Its perturbative formulation appears to be theoretically consistent and agrees with present experiments. Yet, the existence of Adler-Bell-Jackiw anomalies [1] implies that there are also processes that cannot be described by conventional perturbation theory [2]. They give rise to a violation of certain fermionic quantum numbers, notably chirality (Q_5) in (massless) QCD and $B + L$ in QED.

Such anomalous processes are induced by *instantons* [3] which represent tunnelling processes in Yang-Mills gauge theories, associated with the highly degenerate vacuum structure [4].

An experimental discovery of such a novel, non-perturbative manifestation of non-abelian gauge theories would clearly be of basic significance.

A number of results has revived the interest in instanton-induced processes during recent years:

- First of all, it was shown [5, 6] that the generic exponential suppression of these tunnelling rates, $\propto \exp(-4\pi/\alpha)$, may be overcome at *high energies*, mainly due to multi-gauge boson emission in addition to the minimally required fermionic final state.
- A pioneering and encouraging theoretical estimate of the size of the instanton (I) induced contribution to the gluon structure functions in deep-inelastic scattering (DIS) was recently performed in Ref. [7]. It was argued that it is possible to isolate a well-defined and sizable instanton contribution in the regime of small QCD-gauge coupling, on account of the (large) photon virtuality Q^2 . While the instanton-induced contribution to the gluon structure functions turned out to be small at larger values of the Bjorken variable x , it was found in Ref. [7] to increase dramatically towards smaller x .
- Last not least, a systematic phenomenological and theoretical study is under way [8, 9, 10, 11, 12], which clearly indicates that deep-inelastic ep scattering at HERA now offers a unique window to experimentally detect QCD-instanton induced processes through their characteristic final-state signature. The searches for instanton-induced events have just started at HERA and a first upper limit of 0.9 nb at 95% confidence level for the cross-section of QCD-instanton induced events has been placed by the H1 Collaboration [13]. New, improved search strategies are being developed [11] with the help of a Monte Carlo generator (QCDINS 1.3) [9] for instanton-induced events.

In this review, we report on the present status of our broad and systematic study of QCD-instanton induced processes in deep-inelastic scattering [8, 9, 10, 11, 12, 14, 15].

In Sect. 2, we start by summarizing the important theoretical result [12] that instanton-induced processes in deep-inelastic scattering do not suffer from the usually encountered infrared (IR) divergencies associated with the integration over the

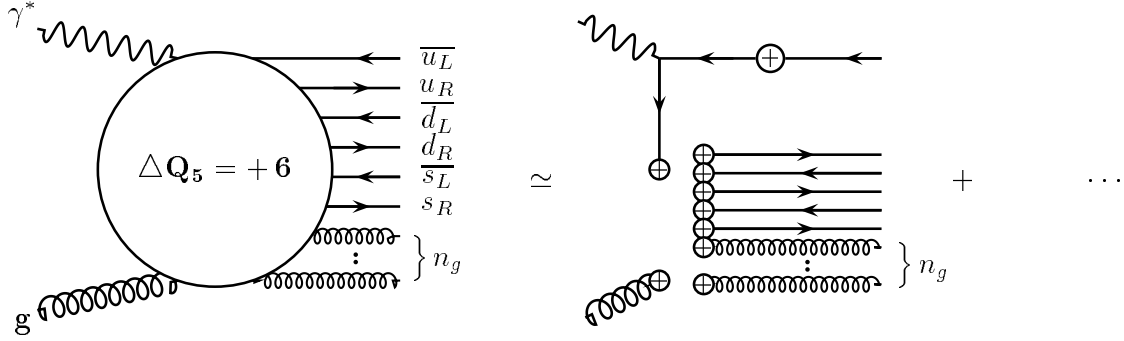


Figure 1: Instanton-induced *chirality-violating* process, $\gamma^* + g \rightarrow \sum_{\text{flavours}}^{n_f} [\bar{q}_L + q_R] + n_g g$, corresponding to three massless flavours ($n_f = 3$).

instanton size. In fact, the inverse hard momentum scale in DIS provides a dynamical IR cutoff for the instanton size. We point out the close analogy of QCD-instanton induced processes in DIS to those in QFD. In Sect. 3, we present the current status of our ongoing theoretical study [14] of the I -induced contribution to deep-inelastic lepto-production. Of interest is, of course, the first (preliminary) estimate of the total I -induced cross-section at HERA. Section 4 is devoted to our phenomenological investigation of the discovery potential for instanton-induced events at HERA by means of a Monte Carlo event generator [9, 15]. The emphasis rests on the study of the characteristic signatures of the final state. We also report on the first searches of instanton-induced events in DIS at HERA. Finally, we discuss improved search strategies, which can serve to enhance the signal from I -induced events relative to the background from normal DIS events.

2 What is Special in Deep-Inelastic Scattering?

As is well known, instanton calculations in QCD are generically plagued by IR divergencies associated with the integration over the instanton size [16]. In this Section, we shall demonstrate explicitly that the typical hard momentum scale Q in deep-inelastic scattering provides a dynamical IR cutoff for the instanton size $\rho_I \lesssim \mathcal{O}(1/Q)$, such that the integration over the size parameter is *finite* [12]. Let us consider the amplitude for the relevant instanton-induced *chirality-violating* photon-gluon process (see Fig. 1),

$$\gamma^* + g \Rightarrow \sum_{\text{flavours}}^{n_f} [\bar{q}_L + q_R] + n_g g ; \quad (\Delta Q_5 \equiv \Delta(Q_R - Q_L) = 2n_f) . \quad (1)$$

The strategy is to first set up the respective Green's function according to standard instanton-perturbation theory in Euclidean space [2, 17, 18, 19, 5], then to Fourier

transform to momentum space, to amputate the external legs, and finally to continue the result to Minkowski space. The basic building blocks are (in Euclidean space and in the singular gauge):

i) The classical instanton gauge field¹ $A_{\mu'}^{(I)}$ [3],

$$A_{\mu'}^{(I)}(x) = -i \frac{2\pi^2}{g_s} \rho_I^2 U_I \left(\frac{\sigma_{\mu'} \bar{x} - x_{\mu'}}{2\pi^2 x^4} \right) U_I^\dagger \frac{1}{\Pi_x}, \quad (2)$$

$$\Pi_x \equiv 1 + \frac{\rho_I^2}{x^2}, \quad (3)$$

depending on the various collective coordinates, the instanton size ρ_I and the colour orientation matrices U_I . The U_I matrices involve both colour and spinor indices, the former ranging as usual only in the 2×2 upper left corner of 3×3 SU(3) colour matrices.

ii) The quark zero modes [2], κ and $\bar{\phi}$,

$$\kappa_{\dot{\beta}}^m(x) = 2\pi \rho_I^{3/2} \epsilon^{\gamma\delta} (U_I)^m_{\delta} \frac{\bar{x}_{\dot{\beta}\gamma}}{2\pi^2 x^4} \frac{1}{\Pi_x^{3/2}}, \quad (4)$$

$$\bar{\phi}_{\dot{\alpha}l}(x) = 2\pi \rho_I^{3/2} \epsilon_{\gamma\delta} (U_I^\dagger)^{\gamma}_{l} \frac{x^{\delta\dot{\alpha}}}{2\pi^2 x^4} \frac{1}{\Pi_x^{3/2}}, \quad (5)$$

and

iii) the quark propagators in the instanton background [17],

$$S^{(I)}(x, y) = \quad (6)$$

$$\frac{1}{\sqrt{\Pi_x \Pi_y}} \left[\frac{x - y}{2\pi^2 (x - y)^4} \left(1 + \rho_I^2 \frac{[U_I x \bar{y} U_I^\dagger]}{x^2 y^2} \right) + \frac{\rho_I^2 \sigma_{\mu}}{4\pi^2} \frac{[U_I x (\bar{x} - \bar{y}) \sigma_{\mu} \bar{y} U_I^\dagger]}{x^2 (x - y)^2 y^4 \Pi_y} \right],$$

$$\bar{S}^{(I)}(x, y) = \quad (7)$$

$$\frac{1}{\sqrt{\Pi_x \Pi_y}} \left[\frac{\bar{x} - \bar{y}}{2\pi^2 (x - y)^4} \left(1 + \rho_I^2 \frac{[U_I x \bar{y} U_I^\dagger]}{x^2 y^2} \right) + \frac{\rho_I^2 \bar{\sigma}_{\mu}}{4\pi^2} \frac{[U_I x \bar{\sigma}_{\mu} (x - y) \bar{y} U_I^\dagger]}{\Pi_x x^4 (x - y)^2 y^2} \right].$$

¹ We use the standard notations, in Euclidean space: $\sigma_{\mu} = (-i\vec{\sigma}, 1)$, $\bar{\sigma}_{\mu} = (i\vec{\sigma}, 1)$, and in Minkowski space: $\sigma_{\mu} = (1, \vec{\sigma})$, $\bar{\sigma}_{\mu} = (1, -\vec{\sigma})$, where $\vec{\sigma}$ are the Pauli matrices. Furthermore, for any four-vector v_{μ} , we use the shorthand $v \equiv v \cdot \sigma$, $\bar{v} \equiv v \cdot \bar{\sigma}$.

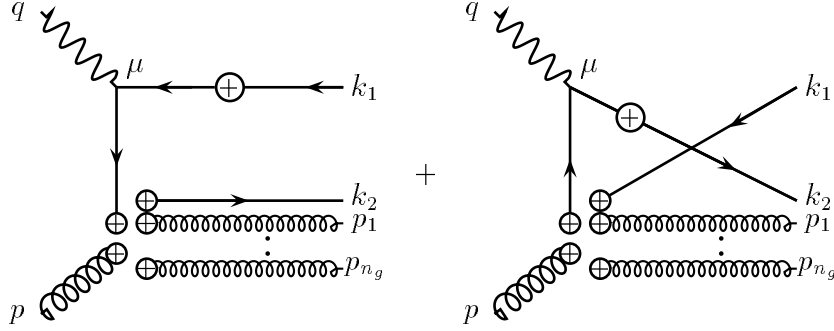


Figure 2: Instanton-induced *chirality-violating* process, $\gamma^* + g \rightarrow \overline{q}_L + q_R + n_g g$, for one massless flavour ($n_f = 1$), in leading semi-classical approximation. The corresponding Green's function involves the products of the appropriate classical fields (lines ending at blobs) as well as the quark propagator in the instanton background (quark line with central blob).

For simplicity, we concentrate here on the case of one flavour ($n_f = 1$ in Eq. (1)), with the generalization to a larger number of flavours being straightforward.

The relevant diagrams for the exclusive process of interest, Eq. (1), are displayed in Fig. 2, in leading semi-classical approximation. The amplitude is expressed in terms of an integral over the collective coordinates ρ_I and the colour orientation U_I ,

$$\mathcal{T}_\mu^{a_1 \dots a_{n_g}} (\gamma^* + g \rightarrow \overline{q}_L + q_R + n_g g) = \quad (8)$$

$$\int dU_I \int_0^\infty \frac{d\rho_I}{\rho_I^5} d(\rho_I, \mu_r) \mathcal{A}_\mu^{a_1 \dots a_{n_g}} (\rho_I, U_I) ; \quad a_{(i)} = 1, 2, 3,$$

where

$$d(\rho_I, \mu_r) = d \left(\frac{2\pi}{\alpha_s(\mu_r)} \right)^6 \exp \left[-\frac{2\pi}{\alpha_s(\mu_r)} \right] (\rho_I \mu_r)^{\beta_0}, \quad (9)$$

denotes the instanton density [2, 18, 19], with μ_r being the renormalization scale. The density (9), with the leading-order expression for $\alpha_s(\mu_r)$,

$$\alpha_s(\mu_r) = \frac{4\pi}{\beta_0 \ln \left(\frac{\mu_r^2}{\Lambda^2} \right)} ; \quad \beta_0 = 11 - \frac{2}{3} n_f, \quad (10)$$

satisfies renormalization-group invariance at the 1-loop level². The constant d is given by

$$d = \frac{C_1}{2} e^{-3C_2 + n_f C_3}, \quad (11)$$

² Two-loop renormalization-group invariance of the density (9) can be achieved [20] by replacing in Eq. (9) β_0 by $\beta_0 + \frac{\alpha_s}{4\pi}(\beta_1 - 12\beta_0)$, with next-to-leading order expression for $\alpha_s(\mu_r)$.

with $C_1 = 0.466$, $C_2 = 1.54$, and $C_3 = 0.153$, in the $\overline{\text{MS}}$ -scheme.

Before analytic continuation, the amplitude \mathcal{A}_μ entering Eq. (8) takes the following form in Euclidean space,

$$\mathcal{A}_\mu^{a_1 \dots a_{n_g}} = -i e_q \lim_{p^2 \rightarrow 0} p^2 \text{tr} \left[\sigma^a \epsilon_g(p) \cdot A^{(I)}(p) \right] \prod_{i=1}^{n_g} \lim_{p_i^2 \rightarrow 0} p_i^2 \text{tr} \left[\sigma^{a_i} \epsilon_g(p_i) \cdot A^{(I)}(-p_i) \right] \times (12)$$

$$\chi_R^\dagger(k_2) \left[\lim_{k_2^2 \rightarrow 0} (ik_2) \kappa(-k_2) \mathcal{V}_\mu^{(t)}(q, -k_1) + \mathcal{V}_\mu^{(u)}(q, -k_2) \lim_{k_1^2 \rightarrow 0} \bar{\phi}(-k_1) (-i \bar{k}_1) \right] \chi_L(k_1),$$

with contributions $\mathcal{V}_\mu^{(t,u)}$ from the diagrams on the left and right in Fig. 2, respectively,

$$\mathcal{V}_\mu^{(t)}(q, -k_1) \equiv \int d^4x e^{-i q \cdot x} \left[\bar{\phi}(x) \bar{\sigma}_\mu \lim_{k_1^2 \rightarrow 0} S^{(I)}(x, -k_1) (-i \bar{k}_1) \right], \quad (13)$$

$$\mathcal{V}_\mu^{(u)}(q, -k_2) \equiv \int d^4x e^{-i q \cdot x} \left[\lim_{k_2^2 \rightarrow 0} (ik_2) \bar{S}^{(I)}(-k_2, x) \sigma_\mu \kappa(x) \right], \quad (14)$$

and generic notation for various Fourier transforms involved,

$$f(\dots, k, \dots) = \int d^4x e^{-i k \cdot x} f(\dots, x, \dots). \quad (15)$$

The four-vector $\epsilon_{g\mu'}$ denotes the gluon polarization-vector, whereas $\chi_{L,R}$ are Weyl-spinors, satisfying the Weyl-equations,

$$\bar{k} \chi_L(k) = 0; \quad k \chi_R(k) = 0, \quad (16)$$

and

$$\chi_L(k) \chi_L^\dagger(k) = k; \quad \chi_R(k) \chi_R^\dagger(k) = \bar{k}. \quad (17)$$

The LSZ-amputation of the classical instanton gauge field $A_{\mu'}^{(I)}$ in Eq. (12) and the quark zero modes κ and $\bar{\phi}$ in Eqs. (13) and (14), respectively, is straightforward [5, 12]. On the other hand, the LSZ-amputation of the quark propagators $S^{(I)}$ and $\bar{S}^{(I)}$ in Eqs. (13) and (14), respectively, is quite non-trivial and involves a lengthy calculation. For the details, we refer the interested reader to Ref. [12]. Here, we only present the final result for the scattering amplitude (8) in Minkowski space,

$$\begin{aligned} \mathcal{T}_\mu^{a_1 \dots a_{n_g}} (\gamma^* + g \rightarrow \bar{q}_L + q_R + n_g g) &= i e_q 4\pi^2 \left(\frac{\pi^3}{\alpha_s} \right)^{\frac{n_g+1}{2}} \int dU_I \int_0^\infty d\rho_I d(\rho_I, \mu_r) \rho_I^{2n_g} \\ &\times \text{tr} \left[\sigma^a U_I [\epsilon_g(p) \cdot p - \epsilon_g(p) \bar{p}] U_I^\dagger \right] \prod_{i=1}^{n_g} \text{tr} \left[\sigma^{a_i} U_I [\epsilon_g(p_i) \bar{p}_i - \epsilon_g(p_i) \cdot p_i] U_I^\dagger \right] \\ &\times \left\{ \left[U_I \chi_R^\dagger(k_2) \epsilon \right] \left[\epsilon V(q, k_1; \rho_I) \bar{\sigma}_\mu \chi_L(k_1) U_I^\dagger \right] \right. \\ &\left. - \left[U_I \chi_R^\dagger(k_2) \sigma_\mu \bar{V}(q, k_2; \rho_I) \epsilon \right] \left[\epsilon \chi_L(k_1) U_I^\dagger \right] \right\}, \end{aligned} \quad (18)$$

where the four-vector V_λ reads

$$V_\lambda(q, k; \rho_I) = \left[\frac{(q - k)_\lambda}{-(q - k)^2} + \frac{k_\lambda}{2q \cdot k} \right] \rho_I \sqrt{-(q - k)^2} K_1 \left(\rho_I \sqrt{-(q - k)^2} \right) \quad (19)$$

$$- \frac{k_\lambda}{2q \cdot k} \rho_I \sqrt{-q^2} K_1 \left(\rho_I \sqrt{-q^2} \right) .$$

At this stage of our instanton calculation, the constraint arising from electromagnetic gauge-invariance,

$$q^\mu \mathcal{T}_\mu^{a a_1 \dots a_{n_g}} = 0 , \quad (20)$$

can easily be checked. Upon contracting (18) with q^μ , it is easy to verify Eq. (20) with the help of the Weyl-equations (16), the relations

$$\sigma_\mu \bar{\sigma}_\nu + \sigma_\nu \bar{\sigma}_\mu = 2 g_{\mu\nu} , \quad (21)$$

of the σ -matrices¹ in Minkowski-space, and the on-shell conditions $k_1^2 = k_2^2 = 0$.

Let us concentrate now on the main objective of this Section: The integration over the instanton size ρ_I in Eq. (18) is *finite* [12]. In particular, the *good infrared* behaviour (large ρ_I) of the integrand is due to the exponential decrease of the Bessel-K function for large ρ_I in Eq. (19),

$$K_1(\mathcal{Q}\rho_I) \xrightarrow{\mathcal{Q}\rho_I \rightarrow \infty} \sqrt{\frac{\pi}{2}} \frac{1}{\sqrt{\mathcal{Q}\rho_I}} \exp[-\mathcal{Q}\rho_I] . \quad (22)$$

Thus, the typical hard scale in deep-inelastic scattering,

$$\mathcal{Q} \equiv \min \left\{ Q \equiv \sqrt{-q^2}, \sqrt{-(q - k_1)^2}, \sqrt{-(q - k_2)^2} \right\} (\geq 0) , \quad (23)$$

provides a dynamical IR cutoff for the instanton size, $\rho_I \lesssim \mathcal{O}(1/\mathcal{Q})$ (at least in leading semi-classical approximation). Therefore, deep-inelastic scattering may be viewed as a distinguished process for studying manifestations of QCD-instantons.

After the integration over the instanton size, which can even be performed analytically [12], we find that the I -induced amplitude (18) is well-behaved as long as we avoid the (collinear) singularities which arise when the internal quark virtualities, $-(q - k_1)^2$ (c.f. Fig. 2 (left)), or $-(q - k_2)^2$ (c.f. Fig. 2 (right)), vanish. Thus, like in perturbative QCD, *fixed-angle scattering processes at high Q^2 and moderate multiplicity are reliably calculable in (instanton) perturbation theory* [12].

Note that the hard scale \mathcal{Q} plays a very similar rôle as the vacuum expectation value of the Higgs field in electro-weak instanton-induced $(B + L)$ -violation [2, 5, 6]. Another close analogy refers to the fact, that, similar to electro-weak instanton-induced $(B + L)$ -violation [5, 6], also QCD-instanton induced processes in DIS are dominated by the multiple production of vector bosons (gluons in the case of QCD;

W 's and Z 's in the case of QFD). This can be seen directly from Eq. (18), since each additional gluon in the final state gives rise to a factor of $(\pi^3/\alpha_s)^{1/2}$ in the amplitude.

In analogy to electro-weak ($B + L$)-violation [6], one expects [7, 8] the sum of the final-state gluon contributions to exponentiate, such that the total I -induced γ^*g cross-section takes the form³ (at large Q^2),

$$\sigma_{\gamma^*g}^{(I)}(x, Q^2) \equiv \sum_{n_g} \sigma_{\gamma^*g n_g}^{(I)}(x, Q^2) \sim \int_x^1 dx' \int_{\mu_f^2}^{Q^2 \frac{x'}{x}} \frac{dQ'^2}{Q'^2} \dots \frac{1}{Q'^2} \exp \left[-\frac{4\pi}{\alpha_s(Q')} F(x') \right], \quad (24)$$

where the so-called ‘‘holy-grail function’’ [6] $F(x')$ (normalized to $F(1)=1$) is expected to decrease towards smaller x' , which implies a dramatic growth of $\sigma_{\gamma^*g}^{(I)}(x, Q^2)$ for decreasing x .

In principle we could verify (24) by exploiting the exclusive amplitudes (18) further, i.e. by performing the collective-coordinate integrations, taking the modulus squared, integrating over the appropriate phase space⁴ and finally summing over n_g . We will, however, adopt a much more powerful method in the next Section which, moreover, will allow us to go beyond the leading semi-classical approximation about the instanton (c.f. Sect. 3.2).

3 Structure Functions and HERA Cross-Section

In this Section we want to concentrate on a first, preliminary estimate of the rate for I -induced events at HERA [14] (subject to appropriate kinematical cuts). Let us recall that, in the one photon exchange approximation, the unpolarized inclusive lepto-production cross-section is parametrized in terms of the familiar structure functions F_2 and F_L ,

$$\frac{d^2\sigma}{dx_{\text{Bj}} dy_{\text{Bj}}} = \frac{4\pi\alpha^2}{Sx_{\text{Bj}}^2 y_{\text{Bj}}^2} \left[\left\{ 1 - y_{\text{Bj}} + \frac{y_{\text{Bj}}^2}{2} \right\} F_2(x_{\text{Bj}}, Q^2) - \frac{y_{\text{Bj}}^2}{2} F_L(x_{\text{Bj}}, Q^2) \right], \quad (25)$$

where \sqrt{S} is the center-of-mass (c.m.) energy of the lepton-hadron system. The Bjorken variables are defined by

$$x_{\text{Bj}} \equiv \frac{Q^2}{2P \cdot q}; \quad y_{\text{Bj}} \equiv \frac{P \cdot q}{P \cdot k}, \quad (26)$$

where $P(k)$ is the four-momentum of the incoming proton (lepton).

³ The lower IR cutoff μ_f^2 in the Q'^2 integration in Eq. (24) serves to regulate the (collinear) divergence mentioned above and plays the rôle of a factorization scale.

⁴ This programme has been performed for the simplest I -induced process, corresponding to $n_f = 1, n_g = 0$, in Ref. [12]. The straightforward generalization is in progress [14].

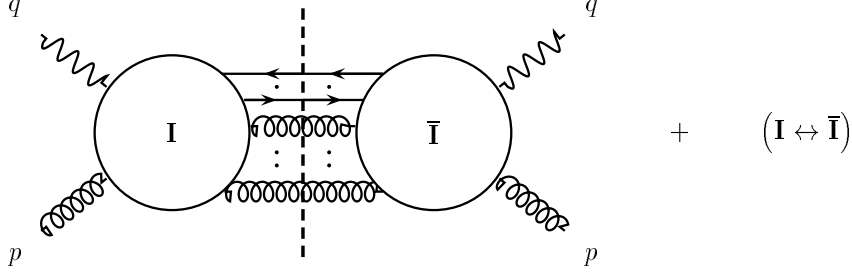


Figure 3: Imaginary part of the $I\bar{I}$ -contribution to the forward γ^*g scattering amplitude.

The I -induced contribution to the nucleon structure functions, e.g. $F_2^{(I)}(x_{\text{Bj}}, Q^2)$, is described [7, 8, 14] in terms of the standard convolution of *parton structure functions*, e.g. $\mathcal{F}_{2g}^{(I)}(x, Q^2)$, with corresponding parton densities, e.g. f_g ,

$$F_2^{(I)}(x_{\text{Bj}}, Q^2) = \sum_{p=q,g} \int_{x_{\text{Bj}}}^1 \frac{dx}{x} f_p\left(\frac{x_{\text{Bj}}}{x}\right) \frac{x_{\text{Bj}}}{x} \mathcal{F}_{2p}^{(I)}(x, Q^2). \quad (27)$$

Let us concentrate next on the calculation of the (dominating) I -induced contribution to the gluon structure functions [14].

3.1 I -Contribution to the Gluon Structure Function

The calculation rests [7, 14] on the optical theorem combined⁵ with the $I\bar{I}$ -valley method [22, 23, 24]. The optical theorem for the virtual $\gamma^*g \rightarrow \gamma^*g$ forward amplitude represents a convenient method to perform implicitly the summation over the I -induced multi-particle final state.

Accordingly, the I -induced contribution to the gluon structure functions can be obtained by simple projections from the imaginary part of the $I\bar{I}$ -contribution to the forward γ^*g scattering amplitude (see Fig. 3),

$$\mathcal{W}_{g\mu\nu}^{(I)}(p, q) = \frac{1}{\pi} \text{Im} \mathcal{T}_{g\mu\nu}^{(I\bar{I})}(p, q) \quad (28)$$

$$\mathcal{F}_{2g}^{(I)}(x, Q^2) = \left[-g^{\nu\mu} + 6x \frac{p^\mu p^\nu}{p \cdot q} \right] x \mathcal{W}_{g\mu\nu}^{(I)}(p, q), \quad (29)$$

⁵ For a combination of the optical theorem with the $I\bar{I}$ -valley method in the context of electro-weak instanton-induced ($B + L$)-violation see Ref. [21].

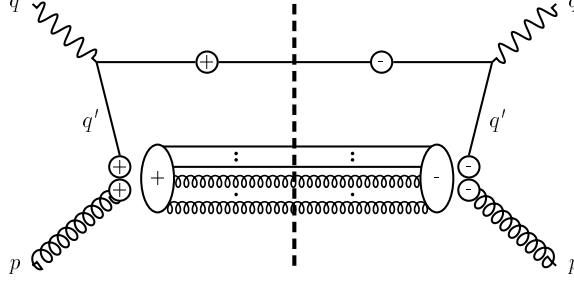


Figure 4: Structure of the imaginary part of the $I\bar{I}$ -contribution to the forward γ^*g scattering amplitude, in leading semi-classical approximation about the $I\bar{I}$ -valley and at large Q^2 .

$$\mathcal{F}_{Lg}^{(I)}(x, Q^2) = 4x^2 \frac{p^\mu p^\nu}{p \cdot q} \mathcal{W}_{g\mu\nu}^{(I)}(p, q), \quad (30)$$

where

$$x \equiv \frac{Q^2}{2p \cdot q} \quad (31)$$

is the Bjorken variable of the γ^*g subprocess.

In order to extract the required $I\bar{I}$ -contribution (c.f. Fig. 3) from the forward γ^*g scattering amplitude, one first evaluates the path-integral expression for the corresponding Green's function in Euclidean space by expanding about the $I\bar{I}$ -configuration $A_\mu^{(I\bar{I})}$ ($I\bar{I}$ “valley”), which is defined via the so-called “valley method” [22, 23, 24]. After Fourier transforming to momentum space, one has to amputate the external legs and to analytically continue to Minkowski space. Finally, the imaginary part is taken.

Along these lines, it is possible to show [14] that, in leading semi-classical approximation about the $I\bar{I}$ -valley and at large Q^2 , the dominant projection contributing to $\mathcal{F}_{2g}(x, Q^2)$ has the following structure (see Fig. 4),

$$\begin{aligned} -g^{\mu\nu} \mathcal{W}_{g\mu\nu}^{(I)}(p, q) &\simeq \sum_q e_q^2 \frac{\pi}{\alpha_s} \int d^4 q' \delta^{(+)}((q - q')^2) \frac{Q^2 (p \cdot q')^2}{((p + q')^2)^{3/2}} \left\{ 1 + \mathcal{O}\left(\frac{Q'^2}{Q^2}\right) \right\} \\ &\times \int dU \int_0^\infty \frac{d\rho_I}{\rho_I^5} \int_0^\infty \frac{d\rho_{\bar{I}}}{\rho_{\bar{I}}^5} \int d^4 R \mathcal{M}(\rho_I, \rho_{\bar{I}}, \xi, U) \exp \left[-\frac{4\pi}{\alpha_s(\mu_r)} S^{(I\bar{I})}(\xi, U) \right] \quad (32) \end{aligned}$$

⁶ For any fixed values of the $I\bar{I}$ collective coordinates τ_i , $\tau = \{\rho_I, \rho_{\bar{I}}, R_\mu, U\}$, the pair configuration $A_\mu^{(I\bar{I})}$ is required to minimize the action within the subspace orthogonal to $\partial A_\mu^{(I\bar{I})} / \partial \tau_i$.

$$\times \exp [i (p + q') \cdot R] K_1 (Q' \rho_I) K_1 (Q' \rho_{\bar{I}}) (\rho_I \rho_{\bar{I}})^{9/2} \left(\frac{16}{\xi^3} \right)^{n_f - \frac{1}{2}},$$

where $Q'^2 \equiv -q'^2$. The second projection (30), entering $\mathcal{F}_{Lg}(x, Q^2)$, may be evaluated analogously [14]. It turns out to vanish in the Bjorken limit.

In analogy to the single instanton case discussed in Sect. 2, the amplitude (32) is expressed in terms of an integral over the appropriate $I\bar{I}$ collective coordinates, the $I(\bar{I})$ -size parameters, $\rho_I(\bar{\rho})$, the distance vector R_μ between I and \bar{I} , and the relative colour orientation, U . Due to conformal invariance of the classical Yang-Mills action, the $I\bar{I}$ -valley action $S^{(I\bar{I})}(\xi, U)$ depends on the distance R_μ and the I - and \bar{I} -sizes only in a conformally invariant manner [22],

$$\xi = \frac{-R^2 + i\epsilon R_0 + \rho_I^2 + \rho_{\bar{I}}^2}{\rho_I \rho_{\bar{I}}}; \quad (\text{in Minkowski space}). \quad (33)$$

The $I\bar{I}$ -valley action itself, for the most attractive relative orientation, $U_0 = \frac{R}{\sqrt{-R^2 + i\epsilon R_0}}$, is given by [23, 24],

$$S^{(I\bar{I})}(\xi, U_0) \equiv \quad (34)$$

$$S^{(I\bar{I})}(\xi) = 1 - \frac{12}{f(\xi)} - \frac{96}{f(\xi)^2} + \frac{48}{f(\xi)^3} [3f(\xi) + 8] \ln \left[\frac{1}{2\xi} (f(\xi) + 4) \right],$$

$$f(\xi) = \xi^2 + \sqrt{\xi^2 - 4}\xi - 4. \quad (35)$$

In Euclidean space, where $-R^2 + i\epsilon R_0$ in (33) is replaced by R^2 , the $I\bar{I}$ -valley action $S^{(I\bar{I})}(\xi)$ corresponds to a smooth interpolation between a widely separated, weakly interacting $I\bar{I}$ -pair configuration ($S^{(I\bar{I})}(\xi \rightarrow \infty) = 1$) and a strongly overlapping one, annihilating to the perturbative vacuum ($S^{(I\bar{I})}(\xi \rightarrow 2) = 0$).

Finally, the combination

$$\mathcal{M}(\rho_I, \rho_{\bar{I}}, \xi, U) \exp \left[-\frac{4\pi}{\alpha_s(\mu_r)} S^{(I\bar{I})}(\xi, U) \right] \simeq \quad (36)$$

$$d^2 \left(\frac{2\pi}{\alpha_s(\mu_r)} \right)^{12} \exp \left[-\frac{4\pi}{\alpha_s(\mu_r)} S^{(I\bar{I})}(\xi, U) \right] (\rho_I \rho_{\bar{I}} \mu_r^2)^{\beta_0 S^{(I\bar{I})}(\xi, U)},$$

appearing in the $I\bar{I}$ -induced amplitude (32), denotes the (one-loop renormalization-group invariant) $I\bar{I}$ -density⁷.

After having defined the quantities entering Eq. (32), let us come now to its physical interpretation. Complementary to the result quoted in Ref. [7], our result

⁷ There are corrections to Eq. (36) which vanish for large ξ . Fortunately, we need the density only at sufficiently large ξ (see below), such that Eq. (36) is approximately valid.

yields a momentum-space picture of the $I\bar{I}$ -contribution to the imaginary part of the forward γ^*g amplitude. As is clear from the discussion in Sect. 2, the $\delta^{(+)}$ -function as well as the Bessel-K functions appearing in Eq. (32) are easily understood as originating from the discontinuity across the handle in the $I\bar{I}$ -induced “handbag” diagram in Fig. 4. The factor $\exp[i(p+q') \cdot R]$, on the other hand, arises from the external gluons $g(p)$ and the internal, virtual quarks $q^*(q')$ in the $I\bar{I}$ background. It is then tempting to introduce the notion of an *I-induced q^*g subprocess*, along with its associated total cross-section [14],

$$\begin{aligned} \sigma_{q^*g}^{(I)}(x', Q^2) &\equiv \frac{8}{3} \frac{\pi^5}{\alpha_s} \frac{Q'^2 (p \cdot q')^2}{((p+q')^2)^{3/2}} \\ &\times \int dU \int_0^\infty \frac{d\rho_I}{\rho_I^5} \int_0^\infty \frac{d\rho_{\bar{I}}}{\rho_{\bar{I}}^5} \int d^4R \mathcal{M}(\rho_I, \rho_{\bar{I}}, \xi, U) \exp \left[-\frac{4\pi}{\alpha_s(\mu_r)} S^{(I\bar{I})}(\xi, U) \right] \\ &\times \exp[i(p+q') \cdot R] K_1\left(\sqrt{Q'^2} \rho_I\right) K_1\left(\sqrt{Q'^2} \rho_{\bar{I}}\right) (\rho_I \rho_{\bar{I}})^{9/2} \left(\frac{16}{\xi^3}\right)^{n_f - \frac{1}{2}}. \end{aligned} \quad (37)$$

Upon partially performing the integration over q'_μ in Eq. (32), one may easily show that, for large Q^2 , the I -contribution to the gluon structure function \mathcal{F}_{2g} , Eq. (29), can be expressed as [14]

$$\mathcal{F}_{2g}^{(I)}(x, Q^2) \simeq \sum_q e_q^2 x \int_x^1 \frac{dx'}{x'} \left(\frac{3}{8\pi^3} \frac{x}{x'} \right) \int_{\mu_f^2}^{Q^2 \frac{x'}{x}} dQ'^2 \sigma_{q^*g}^{(I)}(x', Q'^2), \quad (38)$$

where

$$x' = \frac{Q'^2}{2p \cdot q'} \quad (39)$$

denotes the Bjorken variable of the q^*g subprocess. Thus, in leading-order semi-classical approximation about the $I\bar{I}$ -valley and at large Q^2 , the I -contribution to the gluon structure function \mathcal{F}_{2g} has the form of a convolution of a “splitting function” in the I -background,

$$P_{q^*/\gamma^*}^{(I)}\left(\frac{x}{x'}\right) \equiv \frac{3}{8\pi^3} \frac{x}{x'}, \quad (40)$$

with a total cross-section (37) for the I -induced subprocess, containing the essential instanton dynamics. A generalization of this convolution structure [8] to less inclusive quantities, e.g. single-particle inclusive distributions, is in progress [14].

3.2 The Total Cross-Section of the I -Induced q^*g Subprocess

In this Section we shall concentrate on the most important building block entering Eq. (38), the total cross-section (37) of the I -induced q^*g subprocess (c.f. Fig. 4).

The collective coordinate integrals in Eq. (37) can be done in the saddle-point approximation, the small parameter being $\alpha_s(\mu_r)$. The expression to be extremized is the exponent in Eq. (37),

$$\Gamma(p, q'; \rho_I, \rho_{\bar{I}}, R_\mu, U) \equiv i(p_g + q') \cdot R - Q'(\rho_I + \rho_{\bar{I}}) - \frac{4\pi}{\alpha_s(\mu_r)} S^{(I\bar{I})}(\xi, U), \quad (41)$$

where we have used the asymptotic form (22) for the Bessel-K functions, anticipating that, for small $\alpha_s(\mu_r)$, the dominant contribution to Eq. (37) will come from the region

$$Q' \rho_{I(\bar{I})} \gg 1. \quad (42)$$

The corresponding saddle-point equations are most easily solved in the q^*g c.m. system, where the solution is given by [23, 25],

$$\xi^* = 2 + \frac{4}{\omega'^2}, \quad (43)$$

$$\rho_I^* = \rho_{\bar{I}}^* = \frac{16\pi}{\alpha_s(\mu_r)} \frac{\frac{dS^{(I\bar{I})}}{d\xi}(\xi^*)}{\omega'^2} \frac{1}{Q'}, \quad (44)$$

$$R_\mu^* = \left(-i\sqrt{\rho_I^* \rho_{\bar{I}}^*} \sqrt{\xi^* - 2 - \frac{(\rho_I^* - \rho_{\bar{I}}^*)^2}{\rho_I^* \rho_{\bar{I}}^*}}, \vec{0} \right), \quad (45)$$

$$U^* = \frac{R^*}{\sqrt{-R^{*2}}}. \quad (46)$$

Here ω' denotes a scaling variable corresponding to the q^*g c.m. energy, $\sqrt{s'}$,

$$\omega' \equiv \frac{\sqrt{s'}}{Q'} = \sqrt{\frac{1-x'}{x'}}. \quad (47)$$

Note, that the saddle-point for ρ , Eq. (44), is consistent with our ansatz (42), as long as $\alpha_s(\mu_r)$ is small.

The exponent Γ , Eq. (41), evaluated at the saddle-point, Eqs. (43-46), takes a particularly simple form [23, 25],

$$\Gamma(p, q'; \rho_I^*, \rho_{\bar{I}}^*, R_\mu^*, U^*) = -\frac{4\pi}{\alpha_s(\mu_r)} S^{(I\bar{I})}(\xi^*(x')). \quad (48)$$

It depends only on the scaling variable x' (or, equivalently, on ω').

Now we are ready to perform the integrations about the saddle-point. The final result for the cross-section (37), for small $\alpha_s(\mu_r)$, reads [14],

$$\sigma_{q^*g}^{(I)}(x', Q'^2) \simeq \frac{\Sigma(x')}{Q'^2} \left(\frac{4\pi}{\alpha_s(\mu_r)} \right)^{21/2+2\beta_0 F(x')} \exp \left[-\frac{4\pi}{\alpha_s(Q')} F(x') \right], \quad (49)$$

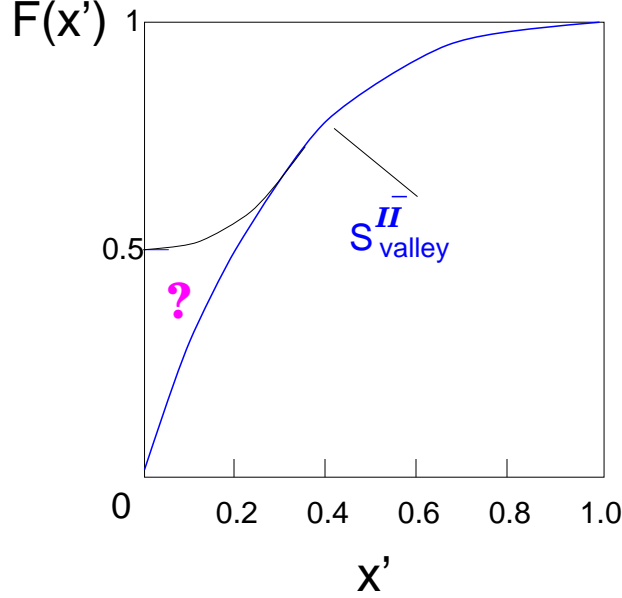


Figure 5: The holy-grail function and the valley action.

where the “holy-grail” function $F(x')$ is here identified as (see Eq. (48) and Fig. 5),

$$F(x') \equiv S^{(I\bar{I})}(\xi^*(x')) . \quad (50)$$

Moreover, we find [14],

$$\Sigma(x') = d^2 \sqrt{6} 2^{n_f-4} \pi^{15/2} \frac{x'^{11/2}}{(1-x')^7} \left(\frac{1-x'}{1+x'} \right)^{3n_f+2} \left[x'(1-x') \frac{dF(x')}{dx'} \right]^{2\beta_0 F(x')-5/2} \quad (51)$$

Let us investigate our result for the holy-grail function $F(x')$, Eq. (50), for small q^*g c.m. energy $\sqrt{s'}$, i.e. small ω' (c.f. Eq. (47)),

$$F(x') = 1 - \frac{3}{8} \left(\frac{1-x'}{x'} \right)^2 + \frac{3}{8} \left(\frac{1-x'}{x'} \right)^3 + \mathcal{O} \left(\left(\frac{1-x'}{x'} \right)^4 \right) . \quad (52)$$

The origin of the different terms on the rhs. of Eq. (52) is illustrated in Fig. 6. The first term (‘t Hooft tunneling factor [2]) corresponds to a purely fermionic final state. The next term arises from the summation of the leading-order gluon emission (c.f. Section 2), and the third term originates [26] from the summation of interference terms between the leading-order gluon emission and the gluon-propagator correction, see Fig. 6.

The $I\bar{I}$ -valley method allows to extrapolate (52) smoothly beyond instanton-perturbation theory, via the identification of the holy-grail function with the $I\bar{I}$ -valley

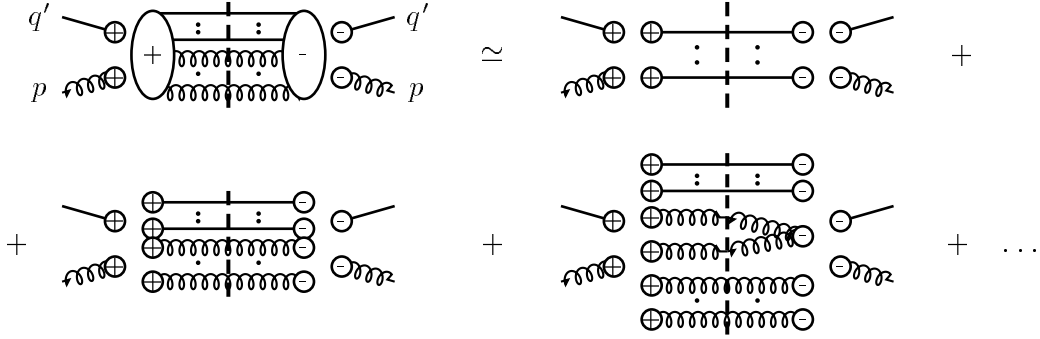


Figure 6: Low-energy expansion of the total instanton-induced subprocess cross-section. The three different graphs on the rhs. correspond to the respective three different terms in the low-energy expansion of the holy-grail function (52).

action at the saddle point, Eq. (50). As we have illustrated in Fig. 6, it effectively sums up the gluonic final-state tree-graph corrections to the leading semi-classical result⁸. However, it has been argued [27] that some initial-state and initial-state - final-state corrections exponentiate as well and might give rise to additional corrections, which show up in the low-energy expansion of the holy-grail function (52) at order $\mathcal{O}(\omega'^5)$. Nevertheless, it appears reasonable to trust our result (49-51) down to $x' = 0.2$, where $F(0.2) \equiv S^{(I\bar{I})}(\xi^*(0.2)) \simeq 1/2$ (see Fig. 5), a value sometimes advocated [28] as the lower bound for the holy-grail function.

As it stands, our result (49) for the I -induced total q^*g cross-section strongly depends on the renormalization scale μ_r . Possible improvements, partly along the lines indicated in footnote 2, will be discussed elsewhere [14]. The main μ_r -dependence in Eq. (49),

$$\left[\frac{4\pi}{\alpha_s(\mu_r)} \right]^{2\beta_0 F(x')} = \left[\beta_0 \ln \left(\frac{\mu_r^2}{\Lambda^2} \right) \right]^{2\beta_0 F(x')}, \quad (53)$$

has its origin in the instanton-size dependence of the $I\bar{I}$ -density (36), $(\rho_I \rho_{\bar{I}} \mu_r^2)^{\beta_0 S^{(I\bar{I})}}$, taken at the saddle point (44). A natural choice [7, 25] for the renormalization scale is $\mu_r = 1/\rho^*$. A closely related choice, which we shall adopt in the following, is to fix the renormalization scale,

$$\mu_r = \mu(Q'), \quad (54)$$

by the requirement,

$$\frac{4\pi}{\alpha_s(\mu(Q'))} \frac{\mu(Q')}{Q'} = 1. \quad (55)$$

⁸ For a formal proof, see first reference in Ref. [26].

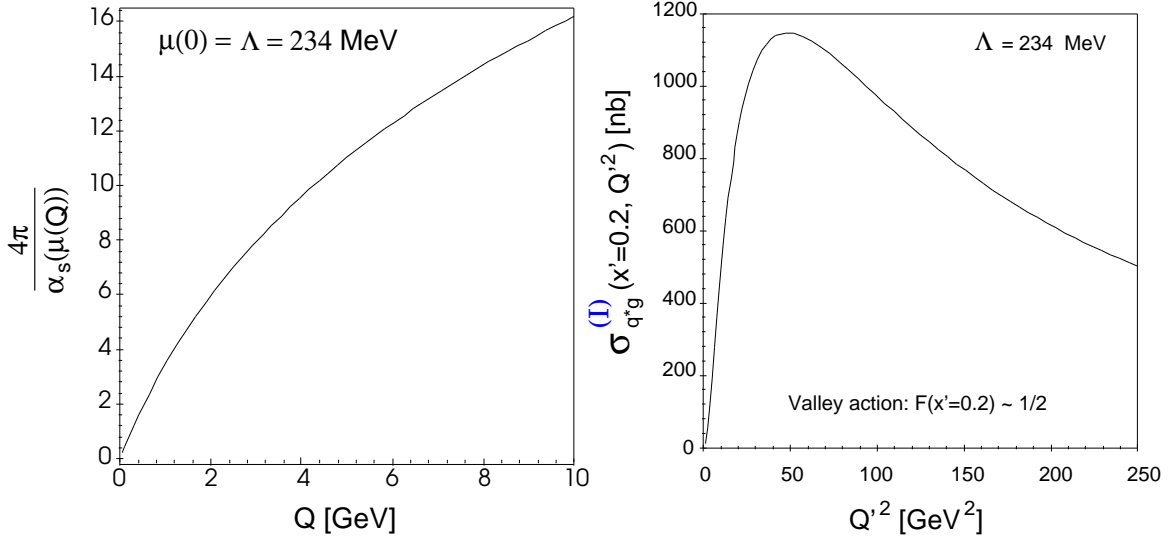


Figure 7: Left: The inverse running coupling at the renormalization scale $\mu(Q)$, acting as the large parameter in the saddle-point approximation. Right: The total cross-section of the I -induced q^*g subprocess, $\sigma_{q^*g}^{(I)}(x', Q'^2)$, for fixed $x' = 0.2$.

With this choice, the cross-section reads [10, 14],

$$\sigma_{q^*g}^{(I)}(x', Q'^2) \simeq \frac{\Sigma(x')}{Q'^2} \left(\frac{4\pi}{\alpha_s(\mu(Q'))} \right)^{21/2} \exp \left[-\frac{4\pi}{\alpha_s(\mu(Q'))} F(x') \right], \quad (56)$$

for $x' \gtrsim 0.2$, $Q' \gtrsim 5$ GeV.

The restriction on x' results mainly from our insufficient knowledge of the holy-grail function $F(x')$ for small x' , whereas the restriction on Q' is due to the requirement that the parameter $4\pi/\alpha_s(\mu(Q'))$ should be large (see Fig. 7 (left)) in order to justify the saddle-point approximation.

Note the following important feature of $\sigma_{q^*g}^{(I)}(x', Q'^2)$, Eq. (56), as a function of Q' (see Fig. 7 (right)): The Q' dependences from the high inverse power⁹ of α_s and the exponential in Eq. (56) compete to produce a strong peak (maximum) far away from the IR region, at a new *hard* scale,

$$\Lambda^{(I)}(x') \equiv 2\beta_0 \frac{\frac{21}{4} - 1}{1 + \beta_0 F(x')} \exp \left\{ \frac{\frac{21}{4} - 1}{1 + \beta_0 F(x')} \right\} \Lambda \gg \Lambda, \quad (57)$$

much above the usual QCD scale Λ . This implies that the I -contribution to the gluon structure function $\mathcal{F}_{2g}^{(I)}(x, Q^2)$, which involves an integration of $\sigma_{q^*g}^{(I)}(x', Q'^2)$ over Q'^2

⁹ The large power 21/2 mainly reflects the number 12 of $\bar{I}\bar{I}$ zero modes minus 1/2 times the number of saddle-point integrations.

(c.f. Eq. (38)),

$$\mathcal{F}_{2g}^{(I)}(x, Q^2) \simeq \sum_q e_q^2 x \int_x^1 \frac{dx'}{x'} P_{q^*/\gamma^*}^{(I)}\left(\frac{x}{x'}\right) \Sigma(x') \quad (58)$$

$$\times \int_{\mu_f^2}^{Q^2 \frac{x'}{x}} \frac{dQ'^2}{Q'^2} \left(\frac{4\pi}{\alpha_s(\mu(Q'))} \right)^{21/2} \exp \left[-\frac{4\pi}{\alpha_s(\mu(Q'))} F(x') \right],$$

is asymptotically dominated by this peak and hence Q independent (scaling) in the Bjorken limit¹⁰,

$$\mathcal{F}_{2g}^{(I)}(x, Q^2) \stackrel{Q \text{ large}}{\approx} \sum_q e_q^2 x \int_x^1 \frac{dx'}{x'} P_{q^*/\gamma^*}^{(I)}\left(\frac{x}{x'}\right) \Sigma(x') 2 \Gamma\left(\frac{21}{2}\right) \frac{F(x') + \frac{21}{4\beta_0}}{F(x')^{23/2}}. \quad (59)$$

The predicted approach to scaling,

$$Q^2 \frac{d\mathcal{F}_{2g}^{(I)}(x, Q^2)}{dQ^2} \stackrel{Q \text{ large}}{\approx} \quad (60)$$

$$\sum_q e_q^2 x P_{q^*/\gamma^*}^{(I)}(1) \frac{\Sigma(x)}{\frac{dF(x)}{dx}} \left[\beta_0 \ln \left(\frac{Q^2}{\Lambda^2} \right) \right]^{\frac{19}{2} + 2\beta_0 F(x)} \left[\frac{\Lambda^2}{Q^2} \right]^{\beta_0 F(x)},$$

resembles a “fractional twist” term, where the twist is sliding with x : the scaling violations vanish faster with increasing x .

Note, however, that the above results for the gluon structure function depend to some extent on our choice of the renormalization scale $\mu_r = \mu(Q')$, Eqs. (54), (55). A thorough investigation of the inherent renormalization- and factorization-scale dependences is presently under way [14]. Then, we may also compare in more detail with the results of Ref. [7] and sort out possible differences.

3.3 HERA Cross-Section

In Fig. 8 we present the resulting I -induced total ep cross-section for HERA, *subject to the following cuts*:

- $x' \geq x'_{\min} = (0.2, 0.3)$ (c.f. discussion in Sec. 3.2) in the integration of Eq. (58);
- $x_{\text{Bj}} \geq x_{\text{Bj min}}, y_{\text{Bj}} \geq 0.1$ in the integration of Eq. (25).

¹⁰Note, that the simplest I -induced (exclusive) process, without gluons in the final state (c.f. Sect. 2), already gives a scaling contribution [12] to the gluon structure function $\mathcal{F}_{2g}^{(I)}(x, Q^2)$.

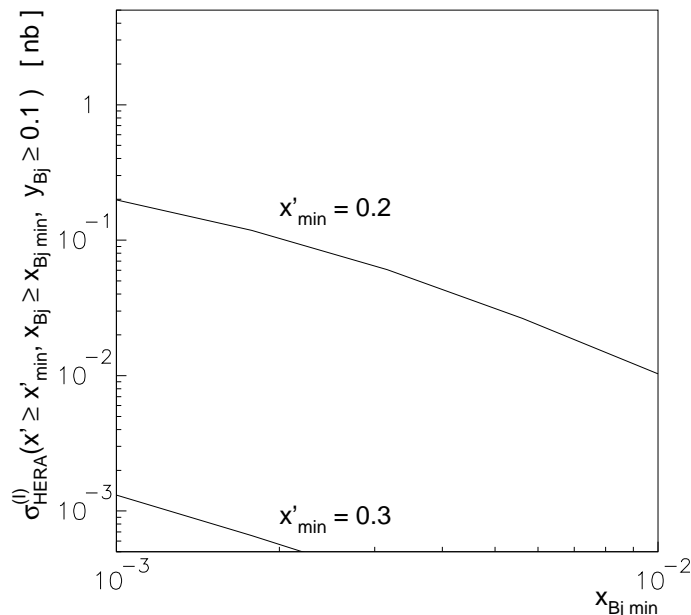


Figure 8: Instanton-induced total ep cross-section for HERA (preliminary) with various cuts as indicated.

So far, only the (dominating) gluon contribution has been taken into account.

Apparently, the cross-section is surprisingly large. Let us, however, emphasize again that the inherent uncertainties associated with the renormalization- and factorization-scale dependences may be considerable [14]. Therefore, Fig. 8 is still to be considered preliminary. Furthermore, there is, of course, also a strong dependence on the precise value of the QCD scale Λ (here taken to be 234 MeV).

4 Monte-Carlo Simulation for HERA

A Monte-Carlo generator for QCD-instanton induced events in DIS, QCDINS 1.3 based on HERWIG 5.8, has been developed¹¹ [9, 15]. It has the following features built-in, which are characteristic for the underlying instanton mechanism:

- In its c.m. system, $\vec{q'} + \vec{p} = 0$, the I -induced multi-parton production is supposed to proceed *isotropically* [2, 5, 6, 7, 10]. We may imagine a “fireball” in S -wave configuration, decaying into gluons and at least $2n_f - 1$ quarks.
- The total parton multiplicity associated with the I -subprocess is large [5, 6, 7,

¹¹ Until the final write-up in Ref. [15] is completed, Ref. [29] may be consulted as a qualitative guide for QCDINS. The Monte-Carlo event generator for electro-weak instanton-induced processes (HERBVI) in Ref. [29] shares a number of similarities with QCDINS.

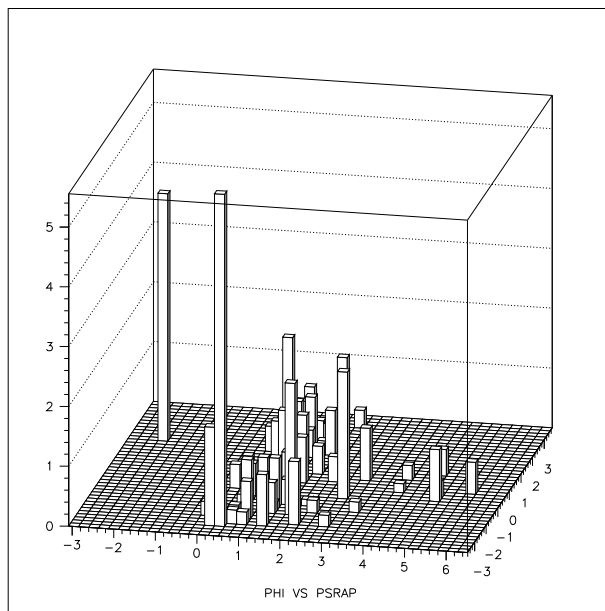


Figure 9: Lego plot $(\eta_{\text{lab}}, \phi_{\text{lab}}, E_T[\text{GeV}])$ of a typical I -induced event in the HERA-lab system at $x_{\text{Bj}} = 10^{-3}$.

10, 14],

$$\langle n_{q+g} \rangle^{(I)} = \mathcal{O}(10) \text{ at HERA.} \quad (61)$$

- The multiplicity distribution at the parton level is taken to be a Poisson distribution¹² [14].
- All light flavours, including strangeness and possibly charm¹³, if kinematically allowed, are democratically produced [2].

At present, we consider the characterization of I -induced events by these final-state features to be more robust than predictions based on cross-section estimates.

The typical event in Fig. 9 from our Monte-Carlo generator [15] illustrates these built-in characteristics: A current-quark jet along with a densely populated hadronic “band” of width $\Delta\eta = \pm 0.9$ in the $(\eta_{\text{lab}}, \phi_{\text{lab}})$ -plane [8]. The band reflects the isotropy in the I -rest system. The total $E_T = \mathcal{O}(20)$ GeV is large as well as the multiplicity, $n_{\text{band}} = \mathcal{O}(25)$. Finally, there is a characteristic flavour flow: All (light) flavours are democratically represented [2] in the final state. Therefore, strongly enhanced rates of K^0 ’s and μ ’s (from strange and charm¹³ decays) in the hadronic band represent crucial signatures for I -induced events.

¹²Strictly speaking, this holds only in the Bjorken limit [14].

¹³ The predictions associated with the I -induced production of charmed quarks are less certain, since for $m_q \rho^* \gtrsim 1$ additional suppression factors may arise.

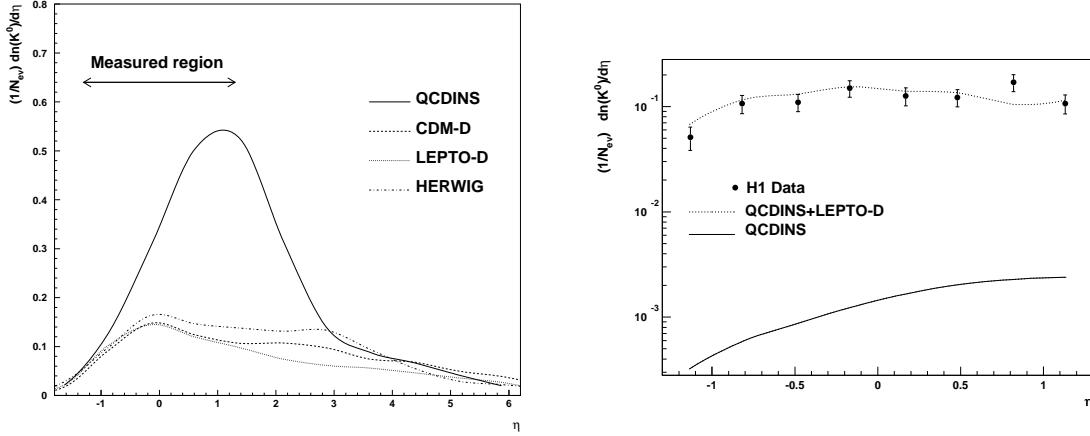


Figure 10: Numbers of K^0 mesons per event with $0.25 < p_T^2 < 4.5 \text{ GeV}^2$ as a function of the HERA-lab pseudorapidity η for the kinematic regime $10 < Q^2 < 70 \text{ GeV}^2$, $10^{-3} < x_{\text{Bj}} < 10^{-2}$, $0.1 < y_{\text{Bj}} < 0.6$. Left: Predictions from various models of (non-diffractive) DIS (broken lines) and from QCDINS (continuous line) for I -induced events only. Right: H1 data (points) with the fit result (dotted line) and the fraction of instanton induced events (solid line), $f = 0.006$, obtained as described in the text. Both figures taken from Ref. [13].

4.1 A First Search for I -Induced Events at HERA

If a significant proportion of DIS events at HERA were induced by QCD-instantons, large changes in the strangeness composition of the hadronic final state would be expected in the “band” region, as illustrated in Fig. 10 (left). This feature of I -induced events has been exploited by the H1 collaboration [13] who searched for an excess in the K^0 rate in the barrel of H1.

They fitted their measured rate of K^0 production, shown as a function of the HERA-lab pseudorapidity η in Fig. 10 (right), with various DIS models, allowing for a fraction f of I -induced events (see Fig. 10 (left)). The largest value of f was obtained using QCDINS with LEPTO [30] and was $f = 0.006 \pm 0.030$. The values f found with different DIS models were all found to be consistent with being zero. Hence, a 95% confidence level upper limit of 0.9 nb was placed [13] on the I -induced cross-section at HERA in the kinematical region considered (c.f. Fig. 10). Note that this limit is less than an order of magnitude above our (preliminary) theoretical estimate presented in Fig. 8, which even contains stronger additional cuts (in particular $x' \geq x'_{\text{min}} = 0.2$).

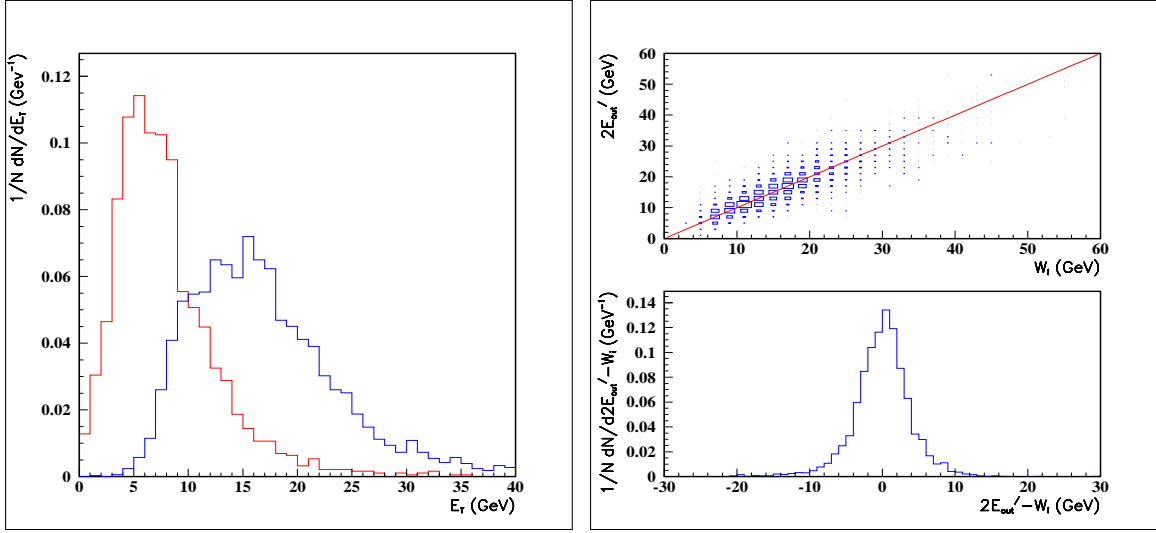


Figure 11: Left: E_T distributions in the γ^*p c.m. system for normal DIS (left) and I -induced events (right). Right: Correlation between $2E_{\text{out}}$ and the I -subprocess c.m. energy $W_I \equiv \sqrt{s'}$. The primes indicate additional cuts in η to minimize next-to-leading-order perturbative QCD effects. Both plots refer to the kinematic region $0.001 < x_{\text{Bj}} < 0.01$, $0.1 < y_{\text{Bj}} < 0.6$ and $20 < Q^2 < 70 \text{ GeV}^2$.

4.2 Improving the Search Strategies

Let us finally mention some recent efforts [11] to improve the sensitivity to I -induced events by adding-in characteristic information on the *event shapes*. The first step consists in boosting to the γ^*p c.m. system and looking for events with high E_T (c.f. Fig. 11 (left)). We note that in this system (1+1) and (2+1) jet¹⁴ perturbative QCD processes deposit their energy predominantly in a *plane* passing through the γ^*p direction. In contrast, the energies from I -induced events are always distributed much more *spherically* (isotropy in the I -rest system!). Therefore, one may substantially reduce the normal DIS background by minimizing (on an event-by-event basis) the quantity

$$E_{\text{out}} = \min_{\hat{i}} \sum_k^n |\vec{p}_k \cdot \hat{i}|, \quad (62)$$

by choice of the unit vector \hat{i} , normal to the γ^*p direction. For standard (2+1) jet events from boson gluon fusion, E_{out} is then only of order of the jet widths. In contrast, for I -induced events, $E_{\text{out}} \simeq \sqrt{s'}/2$ is large (see Fig. 11 (right)). Note, that the peaking of the E_T and $\sqrt{s'} \equiv W_I$ distributions in Fig. 11 around 15 GeV directly reflects the shape of σ_{q^*g} as function of $Q'^2 \propto s'$ (c.f. Fig. 7 (right)). The quantitative results from the Monte-Carlo simulation, subject to additional cuts in η which are

¹⁴As usual in DIS, the +1 refers to the proton remnant.

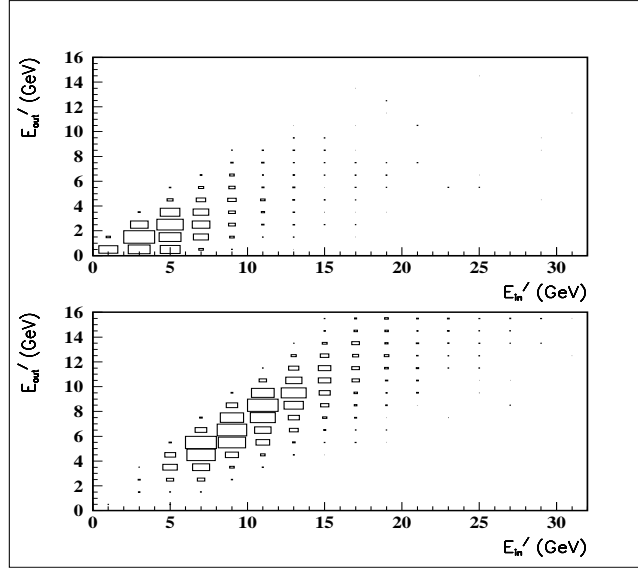


Figure 12: E_{out} vs. E_{in} distributions in the γ^* -proton c.m. system for normal DIS events (top) and I -induced events (bottom) in the kinematic region $0.001 < x < 0.01$, $0.1 < y < 0.6$ and $20 < Q^2 < 70 \text{ GeV}^2$. The primes indicate additional cuts in η to minimize next-to-leading-order perturbative QCD effects.

to minimize higher-order perturbative QCD effects, are displayed in Fig. 12. They fully confirm the qualitative expectations. The power of an I -induced event selection based upon event shape is certainly apparent.

The production of large numbers of partons in the I -subprocess also leads to large charged particle multiplicities in the hadronic final state (c.f. Fig. 9). This is of particular interest for an instanton search, if the HERA detectors can extend their multiplicity measurements to include the region covered by the forward trackers.

Apart from the enhancement of the K^0 production rate, a second feature associated with the flavour democracy of I -induced events is the large number of muons they contain. These result largely from the decay of charmed particles¹³. Unfortunately, their energies are rather low, with the transverse momenta of the muons in the laboratory frame being typically less than 1.5 GeV. Hence, their detection is a challenging task for the experimenters.

Another challenging task is to study, how well the I -subprocess variables s' , x' may be reconstructed/restricted from the hadron momenta in the “band” and the current jet. This would enable us to compare with the theoretical estimates of the production rates which, as explained in Sect. 3.2, are only available in the range $x' \gtrsim 0.2$, $Q' \gtrsim 5 \text{ GeV}$.

5 Conclusions

The experimental discovery of QCD-instanton induced events would clearly be of basic significance, since they correspond to a novel, non-perturbative manifestation of QCD. In addition, they would also provide valuable indirect information about $(B + L)$ -violation in the multi-TeV region, induced by electro-weak instantons.

In this review, we have presented a status report of our broad and systematic study of QCD-instanton induced processes in deep-inelastic scattering [8, 9, 10, 11, 12, 14, 15].

We have emphasized that deep-inelastic scattering may be viewed as a distinguished process for studying manifestations of QCD-instantons, since the available hard scale provides a dynamical infrared cutoff for the instanton size [12]. At high Q^2 , instanton-induced *fixed-angle* processes may be reliably calculated, like in perturbative QCD. Thus, deep-inelastic scattering at HERA offers a unique window to explore footprints of QCD-instantons.

Of great interest is, of course, a first estimate of the total instanton-induced cross-section at HERA. We pursued a complementary approach to Ref. [7], by working out [14] a momentum-space picture of the instanton-contribution to the parton structure functions and further inclusive observables. In leading-order of the semi-classical approximation about the instanton-antiinstanton configuration and at large Q^2 , the instanton-contribution to the gluon structure function \mathcal{F}_{2g} has the form of a convolution of a “splitting function” in the instanton-background with a total cross-section for the instanton-induced q^*g subprocess. The latter contains the essential instanton dynamics. We presented a preliminary theoretical estimate of the total instanton-induced cross-section for deep-inelastic scattering at HERA, subject to appropriate kinematical cuts. Notably, the Bjorken scaling variable of the q^*g subprocess has to be restricted from below, in order to retain theoretical control. Being in the $\mathcal{O}(1-100)$ pb range, the resulting cross-section is surprisingly large. Due to inherent uncertainties associated with the renormalization- and factorization-scale dependencies, which are presently being investigated [14], this cross-section is, however, still to be considered preliminary.

On the phenomenological side, we systematically explored the discovery potential for instanton-induced events at HERA, by studying the characteristics of the final state: A current-quark jet along with a densely populated hadronic “band” of width $\Delta\eta = \pm 0.9$ in the $(\eta_{\text{lab}}, \phi_{\text{lab}})$ -plane, reflecting the *isotropic* decay of an instanton-induced fireball. Characteristic features include the large total transverse energy, $E_T = \mathcal{O}(20)$ GeV, the large multiplicity, $n_{\text{band}} = \mathcal{O}(25)$, and the flavour-democratic production of hadrons, leading in particular to abundant production of K^0 mesons. At present, we consider the characterization of instanton-induced events by these final-state features to be more robust than predictions based on cross-section estimates.

From a recent measurement of K^0 production in deep-inelastic scattering at HERA, the H1 collaboration placed a first upper limit of 0.9 nb (95% confidence

level) on the cross-section for instanton-induced events in the kinematical region considered. This limit is less than an order of magnitude above our (preliminary) theoretical estimate, which even contains stronger additional cuts. We have studied in detail, how a combination of event shape information with searches of K^0 mesons, muons, and multiplicity cuts may further help to discriminate the QCD-instanton induced processes from the standard perturbative QCD background.

Acknowledgements

We would like to acknowledge helpful discussions with V. Braun, V. Rubakov and C. Wetterich.

References

- [1] S. Adler, *Phys. Rev.* **177** (1969) 2426;
J. Bell and R. Jackiw, *Nuovo Cimento* **51** (1969) 47;
W. Bardeen, *Phys. Rev.* **184** (1969) 1848.
- [2] G. 't Hooft, *Phys. Rev. Lett.* **37** (1976) 8; *Phys. Rev. D* **14** (1976) 3432; *Phys. Rev. D* **18** (1978) 2199 (Erratum).
- [3] A. Belavin, A. Polyakov, A. Schwarz and Yu. Tyupkin, *Phys. Lett. B* **59** (1975) 85.
- [4] R. Jackiw and C. Rebbi, *Phys. Rev. Lett.* **37** (1976) 172;
C. Callan, R. Dashen and D. Gross, *Phys. Lett. B* **63** (1976) 334.
- [5] A. Ringwald, *Nucl. Phys. B* **330** (1990) 1;
O. Espinosa, *Nucl. Phys. B* **343** (1990) 310.
- [6] M. Mattis, *Phys. Rep. C* **214** (1992) 159;
P. Tinyakov, *Int. J. Mod. Phys. A* **8** (1993) 1823;
R. Guida, K. Konishi and N. Magnoli, *Int. J. Mod. Phys. A* **9** (1994) 795.
- [7] I. Balitsky and V. Braun, *Phys. Lett. B* **314** (1993) 237.
- [8] A. Ringwald and F. Schrempp, DESY 94-197, hep-ph/9411217, in: *Quarks '94*, Proc. Eighth Int. Seminar, Vladimir, Russia, May 11-18, 1994, eds. D. Gligoriev et al., pp. 170-193.
- [9] M. Gibbs, A. Ringwald and F. Schrempp, DESY 95-119, hep-ph/9506392, in: *Proc. Workshop on Deep Inelastic Scattering and QCD*, Paris, France, April 24-28, 1995, eds. J.-F. Laporte and Y. Sirois, pp. 341-344.

- [10] A. Ringwald and F. Schrempp, DESY 96-125, hep-ph/9607238, to appear in: Proc. Workshop DIS96 on Deep Inelastic Scattering and Related Phenomena, Rome, Italy, April 15-19, 1996.
- [11] M. Gibbs, T. Greenshaw, D. Milstead, A. Ringwald and F. Schrempp, “Search Strategies for Instanton-Induced Processes at HERA”, to appear in Proc. *Future Physics at HERA*, 1996.
- [12] S. Moch, A. Ringwald and F. Schrempp, DESY 96-202, hep-ph/9609445, subm. to Nucl. Phys. B.
- [13] H1 Collaboration, S. Aid et al., DESY 96-122, hep-ex/9607010, subm. to Nucl. Phys.
- [14] S. Moch, A. Ringwald and F. Schrempp, to be published.
- [15] M. Gibbs, A. Ringwald and F. Schrempp, in preparation.
- [16] C. Callan, R. Dashen and D. Gross, *Phys. Rev. D* **17** (1978) 2717;
N. Andrei and D. Gross, *Phys. Rev. D* **18** (1978) 468;
T. Appelquist and R. Shankar, *Phys. Rev. D* **18** (1978) 2952 and references quoted therein.
- [17] L. Brown, R. Carlitz, D. Creamer and C. Lee, *Phys. Rev. D* **17** (1978) 1583.
- [18] C. Bernard, *Phys. Rev. D* **19** (1979) 3013.
- [19] A. Vainshtein, V. Zakharov, V. Novikov and M. Shifman, *Sov. Phys. Usp.* **25** (1982) 195.
- [20] T. Morris, D. Ross and C. Sachrajda, *Nucl. Phys. B* **255** (1985) 115.
- [21] M. Porrati, *Nucl. Phys. B* **347** (1990) 371;
V.V. Khoze and A. Ringwald, *Nucl. Phys. B* **355** (1991) 351;
I. Balitsky and V. Braun, *Nucl. Phys. B* **380** (1992) 51.
- [22] A. Yung, *Nucl. Phys. B* **297** (1988) 47.
- [23] V.V. Khoze and A. Ringwald, *Phys. Lett. B* **259** (1991) 106.
- [24] J. Verbaarschot, *Nucl. Phys. B* **362** (1991) 33;
V.V. Khoze and A. Ringwald, CERN preprint CERN-TH.6082/91 (unpublished).
- [25] I. Balitsky and V. Braun, *Phys. Rev. D* **47** (1993) 1879.

- [26] P. Arnold and M. Mattis, *Phys. Rev. D* **44** (1991) 3650;
 A. Mueller, *Nucl. Phys. B* **364** (1991) 109;
 D. Diakonov and V. Petrov, in: *Proc. of the XXVIth LNPI Winter School*,
 (Leningrad, 1991), pp. 8-64.
- [27] A. Mueller, *Nucl. Phys. B* **348** (1991) 310; *Nucl. Phys. B* **353** (1991) 44.
- [28] V. Zakharov, *Nucl. Phys. B* **353** (1991) 683;
 M. Maggiore and M. Shifman, *Nucl. Phys. B* **365** (1991) 161; *Nucl. Phys. B* **371**
 (1991) 177;
 G. Veneziano, *Mod. Phys. Lett. A* **7** (1992) 1661.
- [29] M. Gibbs, A. Ringwald, B. Webber and J. Zadrozny, *Z. Phys. C* **66** (1995) 285.
- [30] G. Ingelman, in: *Proc. of the Workshop on Physics at HERA*, Hamburg 1991,
 eds. W. Buchmüller and G. Ingelman, Vol. 3, pp. 1366-1394.